Water-Mediated Three-Particle Interactions between Hydrophobic Solutes: Size, Pressure, and Salt Effects

Tuhin Ghosh,[†] Angel E. García,[‡] and Shekhar Garde*[,†]

Department of Chemical Engineering, Rensselaer Polytechnic Institute, Troy, New York 12180 and T-10, Theoretical Biology and Biophysics Group, MS K710 Los Alamos National Laboratory, Los Alamos, New Mexico 87545

Received: September 6, 2002; In Final Form: October 8, 2002

We use molecular dynamics (MD) simulations of solutions of hydrophobic solutes in explicit water to study the many-body character of hydrophobic interactions at the level of solute−solute−solute three-particle correlations. Comparisons of the calculated three-particle potentials of mean force (PMF) with that obtained by adding solute−solute pair PMFs are used to quantify the many-body effect. Our results shed light on both the range and magnitude of many-body (i.e., nonadditivity) effects. We find that the nonadditivity effects depend on the specific configuration of the three interacting particles and are short-ranged, restricted primarily to locations of the third solute within the first two solvation shells of the primary solute pair. The contact and solvent-separated configurations show anticooperative behavior (i.e., the actual three-particle PMF is less favorable than the pairwise additive approximation), whereas cooperativity is observed at the desolvation barrier. Increasing the solute size makes the nonadditive effects uniformly more anticooperative. Nonadditivity behavior is also short-ranged at higher pressures and in NaCl solutions. Interestingly, increasing pressure changes the nonadditivity effects toward cooperativity, whereas the opposite is true upon the addition of salt to the solution. The implications of these results on more complex self-assembly processes are discussed.

I. Introduction

Hydrophobic interactions have continued to be the focus of numerous investigations as a result of their role in important biophysical and colloidal self-assembly phenomena.[1−3] The simplest processes used in fundamental studies of hydrophobic effects, viz., the transfer of a nonpolar molecule into water and the association of a nonpolar solute pair in water, have provided important insights into more complex self-assembly processes[4−17]. For example, the characteristic features of thermal or pressure unfolding of proteins display strong qualitative connections with the temperature and pressure dependence of hydrophobic phenomena at the molecular level.[16,18−26]

Modeling mesoscopic self-assembly processes in aqueous media, however, typically requires a description of *n*-particle free energies (where $n > 2$). For hydrophobic interactions, in particular, this entails connecting the thermodynamics of nonpolar solute hydration and association in dilute aqueous solutions to the formation and stability of hydrophobic aggregates. One of the primary complexities in making such quantitative connections lies in the nonadditivity of hydrophobic interactions; in other words, the free energy of interaction of *n* hydrophobic species (or the *n*-particle PMF) cannot, in general, be expressed as a sum of solute−solute pair PMFs.[13,27−31] The differences between the *n*-particle free energy in a mesoscopic assembly and the pairwise additive description of hydrophobic interactions have been emphasized in earlier studies.[31−35] The inclusion of information on many-body interactions has been shown to lead to collapse or folding processes similar to those observed in experiments.[34,36−38]

The differences between the exact *n*-particle PMF and the pairwise additive approximation (i.e., the cooperative/anticooperative behavior of hydrophobic interactions; see the definition in Methods) have been the subject of several investigations in the recent past. Rank and Baker[13] and Czaplewski et al.[30] considered specific configurations of *n* model solutes in water that are representable along a single reaction coordinate. The *n*-particle PMF evaluated along such a coordinate was compared with the corresponding pairwise additive approximation. The results of Rank and Baker obtained using free-energy perturbation methods indicate anticooperative behavior for hydrophobic interactions. Czaplewski et al.[30] used the weighted histogram analysis method (WHAM)[39] to compute methane PMFs and reported cooperativity for hydrophobic association; the observed differences between the actual free energy and the pairwise additive approximation were, however, small, roughly 10% at short intersolute separations.

More recently, Shimizu and Chan simulated dimers of methane-like solutes in water and evaluated three-particle correlations in the vicinity of the contact pair using test-particle insertion of the third solute.[31] Their results indicate anticooperative character for hydrophobic interactions, with nonadditive behavior extending over a significant range of separations (3−13 Å) between the primary methane dimer and the third methane. Challenges involved in evaluating many-body effects accurately even at the level of three-particle correlations are emphasized by the recent exchange of comments between Czaplewski et al.[40] and Shimizu and Chan.[41] Not only the magnitude and direction of the nonadditivity of pairwise hydrophobic interactions but also the range over which the nonadditivity is significant remain contentious.

Here, we attempt to characterize the many-body nature of hydrophobic interactions at the level of three-particle PMFs.

* To whom correspondence should be addressed. E-mail: gardes@rpi.edu. http://www.rpi.edu/∼gardes.
[†] Rensselaer Polytechnic Institute.
[‡] Los Alamos National Laboratory.

10.1021/jp0220175 CCC: $25.00
Published on Web 12/14/2002

TABLE 1: Partial Charges and Lennard-Jones Interaction Parameters (ϵ and σ) of the Various Atom Types Used in Our MD Simulations

atom	q/e	ϵ (kJ/mol)	σ (Å)
Na	+1.00	0.0619	2.53
Cl	−1.00	0.4429	4.33
Me	0.00	1.2264	3.70
BHS	0.00	1.2264	5.00
O (TIP3P)	−0.834	0.6358	3.15
H (TIP3P)	+0.417	0.00	0.00

TABLE 2: Pressure, NaCl Concentration, and Number of Species of Each Type in the Systems Simulated

no.	P (atm)	N_{solute}	N_{water}	N_{Na^+}	N_{Cl^-}	salt concentration (M)
1	1	10(Me)	508	0	0	0.00
2	1	10(Me)	1016	0	0	0.00
3	1	20(Me)	1016	0	0	0.00
4	1	10(BHS)	508	0	0	0.00
5	4000	10(Me)	508	0	0	0.00
6	4000	10(BHS)	508	0	0	0.00
7	1	10(Me)	518	10	10	1.00
8	1	10(Me)	468	30	30	3.15

We present results from extensive MD simulations of aqueous solutions of hydrophobic solutes in explicit water. Pair and triplet density correlations for model solutes are used to compute two- and three-particle PMFs, respectively. Since we do not rely on archetypical configurations in our calculations, our investigation of the additive/nonadditive character of the free energy of hydrophobic association up to the three-particle level is exhaustive. The general applicability of our results in aqueous solution at 1 atm and 300 K would be contingent upon the sensitivity of the many-body character of hydrophobic interactions to changes in thermodynamic and environment variables. Therefore, we also report many-body effects for changes in two such variables, hydrostatic pressure and the addition of salt (NaCl). Furthermore, simulations of solutions of larger hydrophobic solutes in water shed light on the solute size dependence of many-body effects at the level of solute−solute−solute triplet correlations. The range and magnitude of nonadditive effects reported in this study can provide valuable input to the development of implicit solvent potentials between hydrophobic species.

II. Methods

A. Details of Molecular Dynamics Simulations. Molecular dynamics simulations at constant temperature and pressure were carried out for aqueous solutions of approximately unimolar concentrations of nonpolar solutes using AMBER6.0.[42] Two types of nonpolar solutes were considered—methanes and larger hydrophobic solutes referred to as BHS (see Table 1 for details). Four different simulations of aqueous methane solutions were performed at 1, 4000, and 1 atm with approximately 1 and 3 M NaCl, respectively. Two additional simulations of solutions of larger hydrophobic solutes (BHS) were performed at 1 and 4000 atm. In addition, two simulations of methane solutions were performed with twice the number of waters to estimate system size and methane concentration effects on the calculated pair and triplet correlation functions. Details of these systems are given in Table 2. The TIP3P model[43] was used to represent water molecules explicitly, whereas methanes and the larger hydrophobic solute were represented using a united atom description.[44] The parameters used for Na^+ and Cl^- were those of Straatsma and Berendsen[45] (see Table 1). Lorentz−Berthelotmixing rules were used to model interactions between species of different types.[46]

Periodic boundary conditions were applied, and electrostatic interactions were calculated using the particle-mesh Ewald (PME) method[47] with a grid spacing of approximately 0.8 Å. Bonds in water were constrained using the SHAKE algorithm[48] with a relative geometric tolerance for coordinate resetting of 0.0005 Å. Berendsen's coupling algorithms were used to maintain constant temperature and pressure[49] with the same scaling factor for both solvent and solutes and with the time constant for the heat-bath coupling set at 0.5 ps. The system pressure was regulated using a pressure relaxation time of 0.5 ps in Berendsen's algorithm. A time step of 2 fs was used in all simulations. Equilibration runs were carried out for 1 ns followed by production runs of over 10 ns for each solution; the total simulation time thus exceeds 80 ns.

B. Calculations of Pair and Triplet Correlations. Solute−solute pair correlation functions, $g^{(2)}(r)$'s, were calculated using appropriate normalization volumes.[23,26] These pair correlations were then used to calculate the solute−solute pair PMF, $W^{(2)}(r) = -k_BT \ln g^{(2)}(r)$. Solute−solute−solute triplet correlations were calculated using the method of Krumhansl and Wang.[50] $N^{(3)}(r, s, t)$ denotes the number of solute triplets with the respective solute pair distances between $(r - \Delta/2, r + \Delta/2)$, $(s - \Delta/2, s + \Delta/2)$, and $(t - \Delta/2, t + \Delta/2)$. The solute−solute−solute triplet correlation, $g^{(3)}(r, s, t)$, in a system comprising N_w water molecules and N_S solute particles in a volume V is given by

$$g^{(3)}(r, s, t) = \frac{\langle N^{(3)}(r, s, t)V^2\rangle}{8\pi^2 rst\Delta^3 N_S(N_S - 1)(N_S - 2)}$$

where Δ is the discretization step along the length of each side of the triplet. A discretization step of 0.4 Å was used in our calculations. Appropriate normalization volumes for the evaluation of triplet correlations require that triangle inequalities be accounted for, as discussed in detail earlier.[50,51] Also, triplet correlations are reliable only for (r, s, t) values that satisfy $r + s + t \le L$ where L is the box length.[51] The solute−solute−solute three-particle PMF is then given by $W^{(3)}(r, s, t) = -k_BT \ln g^{(3)}(r, s, t)$. To represent the triplet correlations in a readily understandable form, we plot densities on a square grid in the plane of the first or primary solute pair through the linear interpolation of $g^{(3)}(r, s, t)$ data.

C. Cooperativity/Anticooperativity as Determined from Pair and Triplet Correlations. For a solute−solute−solute triplet configuration (r, s, t) where $r = |\vec{r}_1 - \vec{r}_2|$, $s = |\vec{r}_2 - \vec{r}_3|$, and $t = |\vec{r}_3 - \vec{r}_1|$ denote the respective pair separations between solutes, the three-particle PMF can be expanded as[52]

$$W^{(3)}(r, s, t) = W^{(2)}(r) + W^{(2)}(s) + W^{(2)}(t) + \delta W^{(3)}(r, s, t)$$

Here, we focus on the $\delta W^{(3)}(r, s, t)$ term that quantifies the deviation of a pairwise additive description from the three-particle PMF. The pairwise additive PMF, also known as Kirkwood's superposition approximation (KSA), is given by $(W^{(3)}_{KSA}(r, s, t) = W^{(2)}(r) + W^{(2)}(s) + W^{(2)}(t))$.[52,53] The three-particle interaction is then *cooperative* if $\delta W^{(3)}(r, s, t) < 0$ and *anticooperative* if $\delta W^{(3)}(r, s, t) > 0$.

The solute−solute−solute three-particle correlations were calculated from MD simulations using a bin width of 0.4 Å; bin widths smaller than 0.4 Å yield noisy results. The solute−solute pair correlations can be calculated, however, using much smaller bin widths (0.1 or 0.05 Å). Proper averaging over bin widths needs to be used, therefore, when calculating triplet correlations using KSA that can then be compared with triplet correlations obtained from MD simulations. Such a procedure was followed in this study.

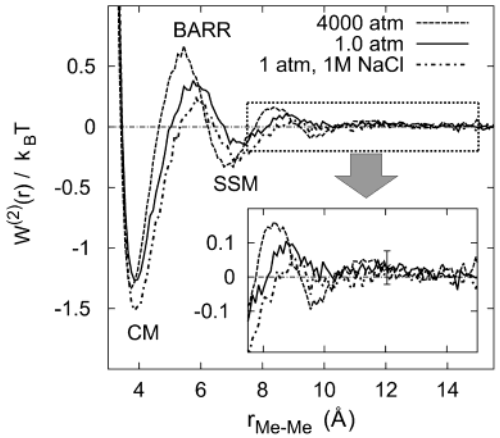

Figure 1. Me−Me pair potentials of mean force obtained from MD simulations at $T = 300$ K and $P = 1$, 4000, and 1 atm with an added NaCl concentration of 1 M. The inset focuses on the behavior at larger Me−Me separations; a typical error bar is also shown.

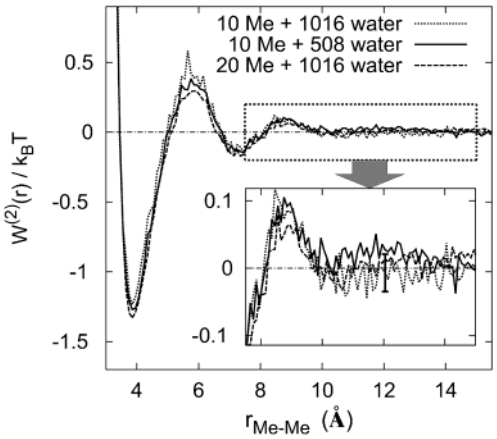

Figure 2. Insensitivity of Me−Me pair PMFs to system size and to methane concentration at $P = 1$ atm and $T = 300$ K.

III. Results and Discussion

A. Methane−Methane Pair Potentials of Mean Force. Figure 1 shows methane−methane pair PMFs in water obtained from MD simulations of aqueous solutions of methanes at 300 K. Although simulations were performed at a variety of thermodynamic conditions for solutions of methanes as well as of larger solutes, only three representative cases are shown. All three Me−Me PMFs in Figure 1 show the contact minimum (CM) in free energy at $r_{Me-Me} \approx 3.9$ Å and the so-called solvent-separated minimum (SSM) at r_{Me-Me} approximately between 7 and 7.5 Å depending on the thermodynamic conditions. The CM and the SSM are separated by a desolvation barrier (BARR) that must be overcome for transitions between the two minima to occur.

The specific effects of hydrostatic pressure and added salt on hydrophobic interactions have been discussed in detail elsewhere.[20,23,26,54] With an increase in hydrostatic pressure from 1 to 4000 atm, an inward movement of the CM, BARR, and SSM configurations is observed. The free energy at CM remains relatively unaffected, the desolvation barrier increases in height, and the free energy at the SSM becomes significantly more favorable. The addition of NaCl has the opposite effect; it increases the tendency of methanes to aggregate in solution, which is reflected in a lowering of the free energy at the CM, SSM, and BARR configurations.

Comparisons of molecular simulation results for two- and three-particle hydrophobic interactions presented here with similar correlation functions obtained from experiments, especially at higher pressures or in the presence of salts or additives, could prove useful for the validation of classical potential models typically employed for complex aqueous mixtures. Soper and coworkers have studied methane−water and methane−methane correlations near clathrate hydrate-forming conditions using neutron-diffraction technique.[55] Qualitatively, their results are consistent with the observations made here and with those reported previously.[19,16,23] In particular, increasing the hydrostatic pressure weakens the strength of hydrophobic interactions and favors solvent-separated configurations.

The long-range behavior of Me−Me pair PMFs is important for the correct interpretation of the nonadditivity of higher-order PMFs. We note that, within statistical uncertainties, all three PMFs shown in Figure 1 approach their correct long-range limit of zero beyond Me−Me separations of approximately 11 Å. Of eight different simulations reported in Table 2, only in two cases is the expected long-range behavior not observed. For a solution of large hydrophobic solutes in water, even in the absence of salt at 1 atm, stronger hydrophobic interactions lead to long-lived aggregates of solutes, leading to nonzero PMFs with positive slopes at larger separations.[23] Similarly, the onset of methane aggregation at higher NaCl concentrations results in nonzero PMF values at larger separations, albeit with zero slope. For the case of 3 M NaCl, we shifted the baseline slightly such that Me−Me pair PMFs approach zero uniformly. Furthermore, as shown in Figure 2, the systems considered here are sufficiently large. The correlations do not change upon doubling the system size or upon changing the concentration of methanes to half its value.

B. Methane−Methane−Methane Triplet Correlations. Figure 3 shows surface plots of Me−Me−Me triplet correlation function $g^{(3)}(\vec{r}_1, \vec{r}_2, \vec{r}_3)$ for three different configurations of the primary methane pair at 1 atm and 300 K. Interestingly, in all three cases, dominant features in the triplet correlations are observed within the first solvation shell of the primary methane pair, whereas only weaker oscillations are seen in the second solvation shell. At locations of the third methane beyond the second solvation shell, the triplet correlations approach values given by KSA. That is, for sufficiently large values of s and t, $g^{(3)}(r, s, t) = g^{(2)}(r)\, g^{(2)}(s)\, g^{(2)}(t) = g^{(2)}(r)$. This observation suggests that the nonadditivity of hydrophobic interactions at the level of triplet correlations is limited to short separations, in agreement with the results of Czaplewski et al.[30,40]

In all three cases, high density of the third methane is localized to two symmetrically placed narrow regions along the Me−Me bisector, allowing the third methane to form contact-like configurations with the primary pair. Particularly interesting features are observed when the primary pair is in the so-called solvent-separated minimum configuration (Figure 3(c). A substantial density of the third methane in the region between the primary pair suggests that the SSM includes both solvent- and solute-separated configurations. Triplet density profiles and their variation with thermodynamic variables are harder to interpret quantitatively through these surface plots. Furthermore, the nonadditivity effects need to be identified through a comparison of $g^{(3)}$ with the density predicted by superposition approximation. Therefore, we consider the intersection of surface plots of triplet density with three different planes—*ABCD*, *KLMN*, and *PQRS* as shown in Figure 4.

The plane *ABCD* intersects the triplet density profile along the bisector. For the CM configuration of the primary methane pair (Figure 4), the region with the highest triplet density occurs along the bisector of the primary methane pair. Corresponding maxima in $g^{(3)}$ at distances of the third methane from the origin

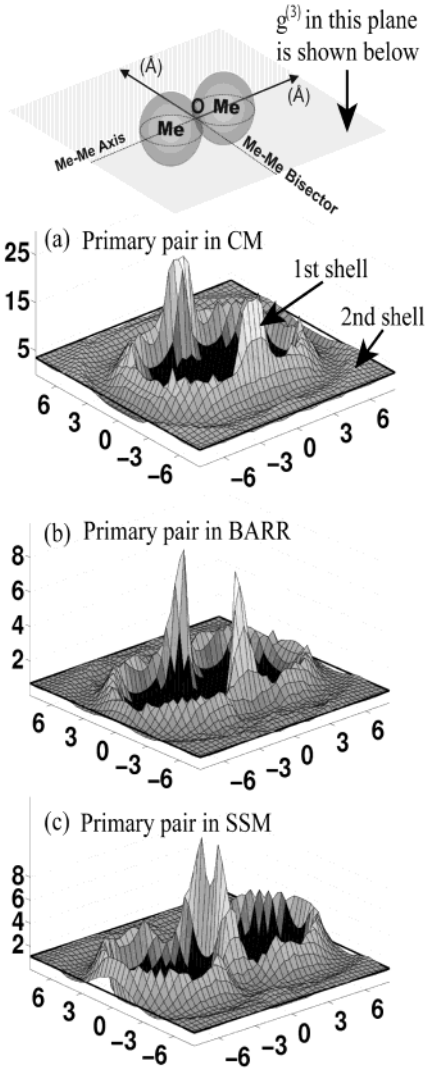

Figure 3. Me−Me−Me triplet correlations obtained from MD simulations at $P = 1$ atm and $T = 300$ K. Surface plots of methane triplet density on a plane containing the methane pair are shown for (a) CM, (b) BARR, and (c) SSM configurations of the primary methane pair. Dark borders in each plot show the long-range (KSA) limit for $g^{(3)}$.

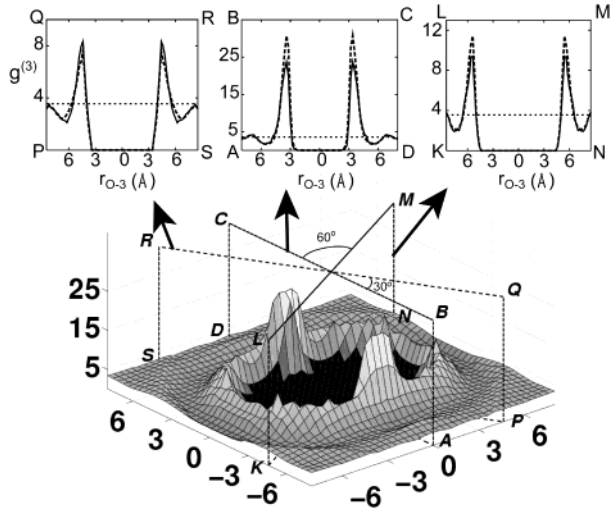

Figure 4. Intersection of the methane triplet density (which is the same as in Figure 3(a)) with planes *ABCD* (along the bisector), *PQRS*, and *KLMN*: projections of the simulation data (—) are compared with values predicted by the superposition approximation (- -).

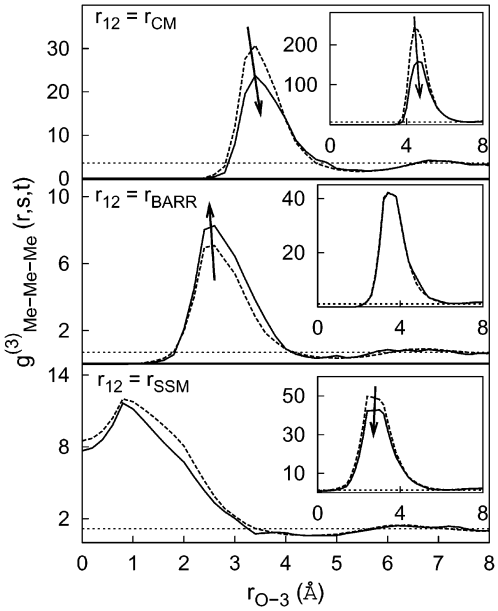

Figure 5. Intersections of the Me−Me−Me triplet density with bisector plane *ABCD* shown in Figure 4 obtained from MD simulations (—) and from KSA (- -) at $P = 1$ atm and $T = 300$ K. The primary methane pair is in CM (top), BARR (middle), and SSM (bottom) configurations. The inset shows triplet correlations for larger BHS solutes. r_{O-3} is the distance of the third methane (or BHS) from the origin "O" along the bisector of the primary pair.

"O", $r_{O-3} = \pm 3.4$ Å, are observed on the plane *ABCD*. The first coordination shell extends up to a distance of $r_{O-3} = \pm 5.5$ Å, and a second maximum in the triplet density is observed at locations corresponding to $r_{O-3} = \pm 7.0$ Å. The locations of both the first and second peak are correctly predicted by KSA, as shown in Figure 4. At separations beyond the first solvation shell, KSA predictions are in excellent agreement with MD results. At shorter separations, especially near the density maxima, KSA overestimates the value of the triplet correlation. As a result, $\delta W^{(3)} = -k_B T \ln[g^{(3)}/g^{(3)}_{KSA}]$ is positive, making the many-body effect at the level of three particles anticooperative.

Similar results are observed along planes *PQRS* and *KLMN*, although slight cooperativity is observed in plane *PQRS*, indicating the conformation dependence of many-body effects. In our subsequent analyses, we focus on the intersection of the triplet density profile with plane *ABCD*.

C. Nonadditivity of Triplet Correlations at $P = 1$ atm and $T = 300$ K for Methanes and Larger Solutes. Figure 5 shows triplet density variations along the bisector of the primary methane pair at 1 atm and 300 K. For all three configurations CM, BARR, and SSM of the primary methane pair, at large distances of the third methane (i.e., large s and t), the triplet correlation approaches the value of the pair correlation for the primary pair, $g^{(2)}(r)$. Deviations from pairwise additivity are observed only at shorter distances, in particular, within the first solvation shell of the primary methane pair.

For CM configurations of the primary methane pair, the most probable location of the third methane is at a distance of ~3.4 Å from the origin O along the bisector, forming an equilateral triangle configuration with $r = s = t \approx 3.9$ Å. For such a configuration, the KSA prediction ($g^{(2)}(r = r_{CM})^3 = 30.7$) is significantly higher than the observed value of 23.7, giving $\delta W^{(3)}_{CM} = +0.26\ k_B T$. The nonadditivity effect is therefore anticooperative. We note here that although the nonadditivity effect for such configurations is anticooperative, direct contact

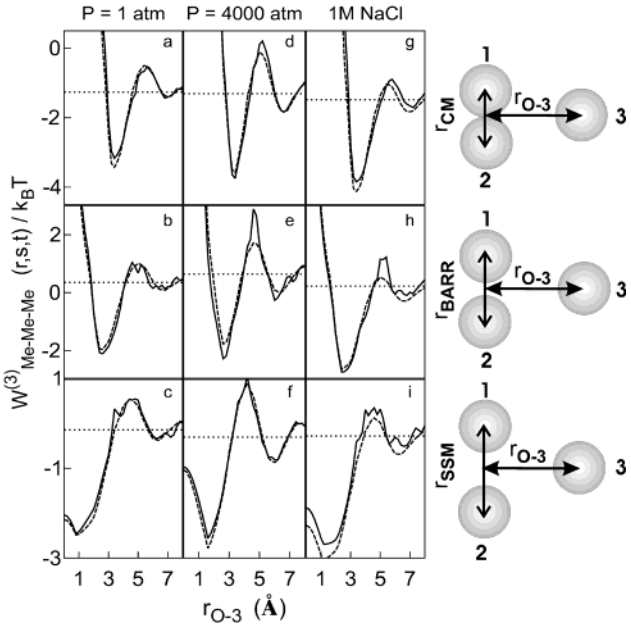

Figure 6. Me−Me−Me three-particle PMFs and $W^{(3)}$ obtained from MD simulations at $P = 1$ (*a*, *b*, *c*) and 4000 atm (*d*, *e*, *f*) and at 1 M NaCl when $P = 1$ atm (*g*, *h*, *i*). Intersections of $W^{(3)}$ with bisector plane *ABCD* are shown for primary Me−Me pair distances corresponding to CM (*a*, *d*, *g*), BARR (*b*, *e*, *h*), and SSM (*c*, *f*, *i*). MD simulation results (—) are compared with KSA values (- -). Dotted horizontal lines represent the exact long-distance limit of $W^{(3)}$ (i.e. $W^{(2)}(r_{12})$).

of three methanes in water is strongly favored, as seen by the high value of $g^{(3)}$. Anticooperativity refers to the fact that the superposition approximation simply overestimates this value somewhat. For BARR configurations of the primary methane pair, in contrast, the triplet density is cooperative in the first solvation shell; $\delta W^{(3)}_{BARR} \approx -0.15\ k_BT$ for $r_{O-3} = 2.6$ Å (Figure 5, middle panel). For SSM configurations of the primary methane pair, the triplet density can be described approximately in terms of KSA ($\delta W^{(3)}_{SSM} \approx 0$) over the entire range of distances along the bisector studied here.

Hydrophobic interactions between larger hydrophobic solutes are stronger than those between methanes both at the pair and triplet level. Indeed, these strong interactions leads to their aggregation at 1 atm. Nevertheless, the nonadditive effects for the larger solutes are similar to those observed for methane triplets (see the insets of Figure 5) and are somewhat enhanced toward anticooperativity ($\delta W^{(3)}_{CM} = +0.4\ k_BT$, $\delta W^{(3)}_{BARR} \approx 0$, and $\delta W^{(3)}_{SSM} = +0.2\ k_BT$) compared to that for methane triplets. Beyond the first coordination shell, however, the actual triplet density conforms well to the superposition approximation. For both sizes of hydrophobic solutes studied, our results suggest that accurate quantitative modeling of three-particle interactions in dilute solution would require the inclusion of nonadditive terms only for short intersolute separations.

D. Effects of Pressure and Salt (NaCl) on Me−Me−Me Triplet PMFs. The nonadditive behavior of Me−Me−Me PMFs observed at short separations of the third methane from the primary methane pair at atmospheric pressure and room temperature, reported in the previous section, need not be a general result and is expected to vary with changes in water structure as a function of thermodynamic conditions. Figure 6 shows the effects of varying two such variables, hydrostatic pressure and the addition of NaCl. High hydrostatic pressure destabilizes hydrophobic aggregates,[16,23,26] whereas the addition of NaCl is known to stabilize folded proteins by favoring hydrophobic association.[56,57]

TABLE 3: Nonadditive Correction to the Three-Particle PMF ($\delta W^{(3)}$) at the Most Probable Location of the Hydrophobic Solute in the Vicinity of a Primary Solute Pair in CM, BARR, and SSM Configurations

solute	P (atm)	NaCl (M)	$\delta W^{(3)}$ (k_BT)		
			CM	BARR	SSM
Me	1	0.0	0.26	−0.15	0.03
Me	4000	0.0	−0.16	−0.51	0.22
Me	1	1.0	0.28	−0.11	0.36
Me	1	3.0	0.49	−0.11	0.36
BHS	1	0.0	0.40	0.0	0.12
BHS	4000	0.0	0.28	−0.06	0.57

In all cases shown in Figure 6, at long distances of the third methane from the primary methane pair, the three-particle PMF approaches its exact limit, $W^{(2)}(r = r_{12})$, as given by KSA. With increasing pressure or salt concentration, changes in the three-particle PMF follow closely those observed previously[23,54] in the pair PMF. Here we focus on the key characteristics of nonadditivity effects. Table 3 lists values of $\delta W^{(3)}$ at the most probable location of the third methane (or BHS) in the vicinity of the primary methane (or BHS) pair for CM, BARR, and SSM configurations of the primary pair. Overall, the CM and SSM configurations are anticooperative, whereas the BARR configurations are mostly cooperative. With increasing pressure, CM and BARR configurations become more cooperative, whereas the SSM configurations become more anticooperative. Similar observations are made for the larger BHS solute triplets. In contrast, the addition of salt makes all three configurations consistently more anticooperative.

As observed earlier for the case of hydrophobic solutes in pure aqueous solution at 1 atm and 300 K, nonadditivity effects are uniformly short-ranged over the thermodynamic conditions reported in this section. The changes in nonadditivity effects resulting from increasing pressure or the addition of salt are equal to or less than $\sim 0.4 k_BT$ (1 kJ/mol at 300 K).

IV. Conclusions

Accurate calculations of *n*-particle ($n > 2$) correlation functions between hydrophobic solutes in aqueous solutions and the subsequent evaluation of nonadditivity effects have remained challenging tasks. Here we have presented such results for hydrophobic solute−solute−solute three-particle correlations in water for two different solute sizes and at different pressures and salt concentrations. Collectively, these results highlight many interesting features of triplet correlation functions. As expected, their additivity/nonadditivity properties depend on the geometric arrangement of the three solutes. Nevertheless, the nonadditivity effects are short-ranged, restricted only to the locations of the third solute in the first solvation shell of the primary pair. The superposition approximation works well beyond the first shell.

Empirically, the sign of the nonadditivity effect (i.e., anti/cooperativity or additivity) appears to be correlated to the strength of the individual pair interactions involved. In general, for hydrophobic solutes, more favorable individual pair interactions tend to overestimate the magnitude of the *n*-particle sum, leading to anticooperativity. For example, although a triplet configuration in which all three solutes are in direct contact is indeed highly favorable, the simple addition of pair PMFs predicts this free energy to be somewhat more favorable, leading to anticooperative behavior ($\delta W^{(3)} > 0$). Simply extending one of the pair distances in that triplet to a barrier configuration reverses the trend—the pairwise addition of the PMFs in this case underestimates the magnitude of the actual PMF, leading to cooperativity. Increasing the solute size or adding salt makes both pair as well as triplet hydrophobic interactions more favorable. As

a result, pairwise approximations of the *n*-particle free energy in these cases tend to overestimate the magnitude of the free energy, leading to more anticooperative behavior. The opposite happens with increasing pressure, which reduces the relative strength of contact configurations with respect to that of the solvent-separated ones thus changing the nonadditivity effects toward cooperativity.

What are the broader implications of these results? Clearly, a quantitative characterization of the deviations of a pairwise additive description from the actual *n*-particle free energy will be critical in the modeling of experimentally observed mesoscopic self-assembly phenomena.[58−61] As a first step, our results provide information that can be used to parametrize implicit solvent potentials[20,62−65] at the three-particle level. Information contained in three-particle correlations between small solutes alone is, however, unlikely to be quantitatively useful for the description of aggregation phenomena involving a large number of solutes[66,67] or the collapse of long polymers,[35] which may be governed by strong dewetting transitions of water. For description of such processes, alternative approaches that include higher-order many-body effects will be required. However, many other problems in biophysics, such as the binding of small ligands to proteins, will directly benefit from the availability of a library of accurate low-order (pair, triplet, etc) water-mediated solute correlations.[11,68] Indeed, such correlations have already been employed in calculations of free energies of molecular association[11] and conformational equilibria of small alkane molecules.[17,64] Studies of pressure, salt, or cosolvent/additive effects on these water-mediated correlations add to the utility of the library of PMFs.

Acknowledgment. We are grateful to Dr. H. S. Ashbaugh for insightful comments on the manuscript. T.G. thanks A. Kalra for help with the MD simulations. We are grateful for financial support from an NSF CAREER award (CTS-0134023) for S.G. and for partial support from an ACS-PRF 37664-G7 grant. A.E.G. acknowledges financial support through LDRD grant 2001013ER.

References and Notes

(1) Kauzmann, W. *Adv. Protein Chem.* **1959**, *14*, 1.
(2) Tanford, C. *The Hydrophobic Effect: Formation of Micelles and Biological Membranes;* John Wiley: New York, 1973.
(3) Dill, K. A. *Biochemistry* **1990**, *29*, 7133.
(4) Ben-Naim, A. *Hydrophobic Interactions;* Plenum Press: New York, 1980.
(5) Pratt, L. R.; Chandler, D. *J. Chem. Phys.* **1977**, *67*, 3683.
(6) Privalov, P. L.; Gill, S. J. *Adv. Protein Chem.* **1988**, *39*, 191.
(7) Smith, D. E.; Haymet, A. D. J. *J. Chem. Phys.* **1993**, *98*, 6445.
(8) Wallqvist, A.; Berne, B. J. *J. Phys. Chem.* **1995**, *99*, 2885.
(9) Wallqvist, A.; Berne, B. J. *J. Phys. Chem.* **1995**, *99*, 2893.
(10) Ludemann, S.; Schreiber, H.; Absher, R.; Steinhauser, O. *J. Chem. Phys.* **1996**, *104*, 286.
(11) Garde, S.; Hummer, G.; Paulaitis, M. E. *Faraday Discuss.* **1996**, *103*, 125.
(12) Ludemann, S.; Absher, R.; Schreiber, H.; Steinhauser, O. *J. Am. Chem. Soc.* **1997**, *119*, 4206.
(13) Rank, J. A.; Baker, D. *Protein Sci.* **1997**, *6*, 347.
(14) Hummer, G.; Garde, S.; Garcıa, A. E.; Pohorille, A.; Pratt, L. R. *Proc. Natl. Acad. Sci. U.S.A.* **1996**, *93*, 8951.
(15) Hummer, G.; Garde, S.; Garcıa, A. E.; Paulaitis, M. E.; Pratt, L. R. *J. Phys. Chem. B.* **1998**, *102*, 10469.
(16) Hummer, G.; Garde, S.; García, A. E.; Paulaitis, M. E.; Pratt, L. R. *Proc. Natl. Acad. Sci. U.S.A.* **1998**, *95*, 1552.
(17) Ashbaugh, H. S.; Garde, S.; Hummer, G.; Kaler, E. W.; Paulaitis, M. E. *Biophys. J.* **1999**, *100*, 1900.
(18) Garde, S.; Hummer, G.; García, A. E.; Paulaitis, M. E.; Pratt, L. R. *Phys. Rev. Lett.* **1996**, *77*, 4966.
(19) Payne, V. A.; Matubayasi, N.; Murphy, L. R.; Levy, R. M. *J. Phys. Chem. B* **1997**, *101*, 2054.
(20) Hillson, N.; Onuchic, J. N.; García, A. E. *Proc. Natl. Acad. Sci. U.S.A.* **1999**, *96*, 14848.
(21) Huang, D. M.; Chandler, D. *Proc. Natl. Acad. Sci. U.S.A.* **2000**, *97*, 8324.
(22) Silva, J. L.; Foguel, D.; Royer, C. A. *Trends Biochem. Sci.* **2001**, *26*, 612.
(23) Ghosh, T.; García, A. E.; Garde, S. *J. Am. Chem. Soc.* **2001**, *123*, 10997.
(24) Garde, S.; Ashbaugh, H. S. *J. Chem. Phys.* **2001**, *115*, 977.
(25) Ashbaugh, H. S.; Truskett, T. M.; Debenedetti, P. G. *J. Chem. Phys.* **2002**, *116*, 2907.
(26) Ghosh, T.; García, A. E.; Garde, S. *J. Chem. Phys.* **2002**, *116*, 2480.
(27) Bruge, F.; Fornili, S. L.; Malenkov, G. G.; Palma-Vittorelli, M. B.; Palma, M. U. *Chem. Phys. Lett.* **1996**, *254*, 283.
(28) Pellegrini, M.; Grønbech-Jensen, N.; Doniach, S. *J. Chem. Phys.* **1996**, *104*, 8639.
(29) Martorana, V.; Bulone, D.; Biagio, P. L. S.; Palma-Vittorelli, M. B.; Palma, M. U. *Biophys. J.* **1997**, *73*, 31.
(30) Czaplewski, C.; Rodziewicz-Motowidlo, S.; Liwo, A.; Ripoll, D. R.; Wawak, R. J.; Scheraga, H. A. *Protein Sci.* **2000**, *9*, 1235.
(31) Shimizu, S.; Chan, H. S. *J. Chem. Phys.* **2001**, *115*, 1414.
(32) Wood, R. H.; Thompson, P. T. *Proc. Natl. Acad. Sci. U.S.A.* **1990**, *87*, 946.
(33) Lum, K.; Chandler, D.; Weeks, J. D. *J. Phys. Chem. B* **1999**, *103*, 4570.
(34) Chan, H. S. *Proteins: Struct., Funct., Genet.* **2000**, *40*, 543.
(35) ten Wolde, P. R.; Chandler, D. *Proc. Natl. Acad. Sci. U.S.A.* **2002**, *99*, 6539.
(36) Sorenson, J. M.; Head-Gordon, T. *Folding Des.* **1998**, *3*, 523.
(37) Plotkin, S. S.; Wang, J.; Wolynes, P. G. *J. Chem. Phys.* **1997**, *106*, 2932.
(38) Dill, K. A. *J. Biol. Chem.* **1997**, *272*, 701.
(39) Kumar, S.; Rosenberg, J. M.; Bouzida, D.; Swendsen, R. H.; Kollman, P. A. *J. Comput. Chem.* **1995**, *16*, 1339.
(40) Czaplewski, C.; Rodziewicz-Motowidlo, S.; Liwo, A.; Ripoll, D. R.; Wawak, R. J.; Scheraga, H. A. *J. Chem. Phys.* **2002**, *116*, 2665.
(41) Shimizu, S.; Chan, H. S. *J. Chem. Phys.* **2002**, *116*, 2668.
(42) Pearlman, D. A.; Case, D. A.; Caldwell, J. W.; Ross, W. S.; Cheatham, T. E.; Debolt, S.; Ferguson, D.; Seibel, G.; Kollman, P. *Comput. Phys. Commun.* **1995**, *91*, 1.
(43) Jorgensen, W. L.; Chandrashekhar, J.; Madura, J. D.; Impey, R. W.; Klein, M. L. *J. Chem. Phys.* **1983**, *79*, 926.
(44) Jorgensen, W. L.; Tirado-Rives, J. *J. Am. Chem. Soc.* **1988**, *110*, 1657.
(45) Straatsma, T. P.; Berendsen, H. J. C. *J. Chem. Phys.* **1988**, *89*, 5876.
(46) Allen, M. P.; Tildesley, D. J. *Computer Simulation of Liquids;* Clarendon Press: Oxford, U.K., 1987.
(47) Darden, T.; York, D.; Pedersen, L. *J. Chem. Phys.* **1993**, *98*, 10089.
(48) Ryckaert, J. P.; Ciccotti, G.; Berendsen, H. J. C. *J. Comput. Phys.* **1977**, *23*, 327.
(49) Berendsen, H. J. C.; Postma, J. P. M.; van Gunsteren, W. F.; DiNola, A.; Haak, J. R. *J. Chem. Phys.* **1984**, *81*, 3684.
(50) Krumhansl, J. A.; Wang, S. *J. Chem. Phys.* **1972**, *56*, 2034.
(51) Hummer, G.; Soumpasis, D. M. *J. Chem. Phys.* **1993**, *98*, 581.
(52) Hill, T. L. *An Introduction to Statistical Thermodynamics;* Addison-Wesley: Reading, MA, 1960.
(53) Kirkwood, J. G. *J. Chem. Phys.* **1935**, *3*, 300.
(54) Kalra, A.; Ghosh, T.; Garde, S. To be submitted for publication.
(55) Koh, C. A.; Wisbey, R. P.; Wu, X.; Westacott, R. E.; Soper, A. K. *J. Chem. Phys.* **2000**, *113*, 6390.
(56) Collins, K. D. *Biophys. J.* **1997**, *72*, 65.
(57) Kalra, A.; Tugcu, N.; Cramer, S. M.; Garde, S. *J. Phys. Chem. B* **2001**, *105*, 6380.
(58) Bryson, J. W.; Betz, S. F.; Lu, H. S.; Suich, D. J.; Zhou, H. X.; O'Neil, K. T.; DeGrado, W. F. *Science (Washington, D.C.)* **1995**, *270*, 935.
(59) Stupp, S. I.; LeBonheur, V.; Walker, K.; Li, L. S.; Huggins, K. E.; Keser, M.; Amstutz, A. *Science (Washington, D.C.)* **1997**, *276*, 384.
(60) Nelson, J. C.; Saven, J. G.; Moore, J. S.; Wolynes, P. G. *Science (Washington, D.C.)* **1998**, *277*, 1793.
(61) Klein-Seetharaman, J.; Oikawa, M.; Grimshaw, S. B.; Wirmer, J.; Duchardt, E.; Ueda, T.; Imoto, T.; Smith, L. J.; Dobson, C. M.; Schwalbe, H. *Science (Washington, D.C.)* **2002**, *295*, 1719.
(62) Roux, B.; Simonson, T. *Biophys. Chem.* **1999**, *78*, 1.
(63) Massova, I.; Kollman, P. A. *J. Am. Chem. Soc.* **1999**, *121*, 8133.
(64) Hummer, G. *J. Am. Chem. Soc.* **1999**, *121*, 6299.
(65) Cheung, M. S.; García, A. E.; Onuchic, J. N. *Proc. Natl. Acad. Sci. U.S.A.* **2002**, *99*, 685.
(66) Raschke, T. M.; Tsai, J.; Levitt, M. *Proc. Natl. Acad. Sci. U.S.A.* **2001**, *98*, 5965.
(67) Shimizu, S.; Chan, H. S. *J. Chem. Phys.* **2001**, *115*, 3424.
(68) Siebert, X.; Hummer, G. *Biochemistry* **2002**, *41*, 2956.